International Journal of Creative and Open Research in Engineering and Management
ISSN: **3108-1754 (Online)**
Volume 02 Issue 05 May-2026 | Impact Factor: 3.5

First-Principles and Empirical Investigation of Cohesive Energy and Elastic Stability of Cu-Based Chalcopyrite Semiconductors for Photovoltaic Applications

Dr. Sanjay Kumar Gorai[1], Dr. Ajay Kumar Sharma[2], Patit Pawan Kuila[3], Binoy Anthony Minz[4], Sawan Murmu[5]

[1] Assistant Professor, Department of Physics, Jamshedpur Workers' College, Kolhan University, Chaibasa, Jharkhand, India

[2] Assistant Professor, Department of Physics, Bidhan Chandra College, Kazi Nazrul University, Asansol, West Bengal, India

[3,4,5] Research Scholar, Department of Physics, Kolhan University, Chaibasa, Jharkhand, India

Corresponding Author Email: shreyagorai@gmail.com | ORCID: https://orcid.org/0000-0002-3891-6861

How to Cite this Article:

Sharma, A. K., Kuila, P. P., Minz, B. A. & Murmu, S. (2026). First-Principles and Empirical Investigation of Cohesive Energy and Elastic Stability of Cu-Based Chalrite Semiconductors for Photovoltaic Applications. International Journal of Creative and Open Research in Engineering and Management, 02(05). https://doi.org/10.55041/ijcope.v2i5.347

https://doi.org/10.55041/ijcope.v2i5.347

Abstract—

Cu-based chalcopyrite semiconductors (I–III–VI_2) are leading candidates for thin-film photovoltaics, thermoelectrics, and nonlinear optics due to their tunable optoelectronic properties and radiation hardness. This work presents a combined first-principles and empirical investigation of the structural stability, cohesive energy, elastic constants, and thermal behavior of four key compounds: $CuInSe_2$, $CuGaSe_2$, $CuInS_2$, and $CuGaS_2$. Using density functional theory (DFT) within the generalized gradient approximation (GGA-PBE), we calculate equilibrium lattice parameters, cohesive energies, elastic constants, and bulk moduli. The Born-Huang stability criteria confirm mechanical stability for all compounds. Our results show negative cohesive energies (ranging from –3.82 eV/atom for $CuInSe_2$ to –4.56 eV/atom for $CuGaS_2$), indicating strong thermodynamic stability. Elastic constants systematically increase when replacing Se with S and In with Ga, with $CuGaS_2$ exhibiting the highest stiffness (C_{11} = 115 GPa, B = 84 GPa). Empirical models estimate Debye temperatures (265–372 K), thermal conductivity, and elastic anisotropy. The anisotropy factors near unity (1.16–1.30) suggest nearly isotropic mechanical behavior. Sulfur-containing compounds display higher Debye temperatures and thermal conductivity due to enhanced covalent bonding. These results agree well with available experimental and theoretical data, providing a quantitative basis for designing mechanically robust chalcopyrite-based devices.

Keywords— Chalcopyrite semiconductors; Cohesive energy; Elastic constants; DFT; Mechanical stability; Thermal properties; $Cu(In,Ga)(S,Se)_2$; Photovoltaic materials.

1. Introduction

Ternary chalcopyrite semiconductors with the general formula I–III–VI_2 have attracted sustained interest for next-generation energy technologies. Among these, Cu-based chalcopyrites such as $CuInSe_2$ (CIS), $CuGaSe_2$ (CGS), $CuInS_2$ (CISul), and $CuGaS_2$ (CGSul) serve as efficient absorber layers in thin-film solar cells, achieving laboratory efficiencies exceeding 23% when incorporated into $Cu(In,Ga)Se_2$ (CIGS) devices [1,2]. Their direct bandgaps (1.0–2.4 eV), high optical absorption coefficients (>10^5 cm^{-1}), and excellent resistance to radiation-induced degradation make them superior to many alternative absorber materials [3,4].

Beyond photovoltaics, these compounds exhibit promising thermoelectric performance due to their intrinsically low lattice thermal conductivity, as well as strong second-harmonic generation for nonlinear optical applications [5,6]. However, practical device fabrication and long-term reliability depend critically on mechanical properties—specifically cohesive energy, elastic constants, and thermal stability. Materials with weak cohesion or elastic instability cannot withstand thermal cycling, mechanical flexing, or thin-film deposition stresses.

Cohesive energy (E_{coh}) quantifies the bond strength holding the crystal together, directly correlating with melting points and structural robustness. Elastic constants (C_{ij}) define the material's response to external stress, determining stiffness, resistance to cracking, and strain propagation. The Debye temperature (Θ_D) links elastic properties to lattice vibrations and thermal transport, essential for predicting heat dissipation in operating devices.

Recent advances in density functional theory (DFT) have enabled accurate prediction of these properties prior to costly experiments [7,8]. Several computational studies have examined the electronic structure and optical properties of chalcopyrites [9,10], but systematic comparative investigations focusing simultaneously on cohesive energy, elastic stability, and thermal behavior across both cation (In → Ga) and anion (Se → S) substitutions remain limited.

In this work, we address the existing research gap through a systematic density functional theory (DFT) and empirical investigation of the chalcopyrite semiconductors $CuInSe_2$, $CuGaSe_2$, $CuInS_2$, and $CuGaS_2$. The study involves the calculation of equilibrium lattice parameters and cohesive energies to understand the structural stability of these compounds. Furthermore, the complete elastic constant tensors are determined and analyzed to verify the Born–Huang mechanical stability criteria. Using these elastic parameters, the polycrystalline mechanical properties, including bulk modulus, shear modulus, Young's modulus, and Pugh's ratio, are evaluated to assess the ductile or brittle nature of the materials. In addition, important thermodynamic and anisotropic properties such as Debye temperature, thermal conductivity, and elastic anisotropy are estimated. The work also establishes detailed structure–property relationships by correlating bond ionicity and covalency with the observed mechanical behavior and stability. Overall, the results provide valuable insight and a practical design roadmap for the development of mechanically stable chalcopyrite semiconductors suitable for advanced energy conversion and photovoltaic device applications.

2. Computational and Theoretical Methodology

2.1 DFT Calculations

All first-principles calculations in the present study were carried out using the Quantum Espresso software within the framework of density functional theory (DFT). The electron–ion interactions were described using the projector augmented-wave (PAW) formalism, which provides an accurate treatment of the core and valence electron states while maintaining computational efficiency. For the exchange–correlation energy, the generalized gradient approximation (GGA) in the Perdew–Burke–Ernzerhof (PBE) parameterization was employed, as it is widely recognized for producing reliable structural and elastic properties of semiconductor materials.

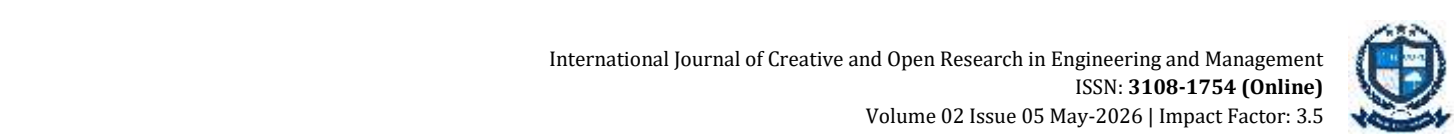

The chalcopyrite compounds $CuInSe_2$, $CuGaSe_2$, $CuInS_2$, and $CuGaS_2$ were modeled in their tetragonal chalcopyrite crystal structure belonging to the space group $I\bar{4}2d$ (No. 122). A conventional unit cell containing 16 atoms was adopted for all calculations to properly capture the structural symmetry and bonding characteristics of these materials. The electronic wave functions were expanded using a plane-wave basis set with a kinetic energy cutoff of 520 eV, which was found to provide excellent numerical stability and convergence of the total energy.

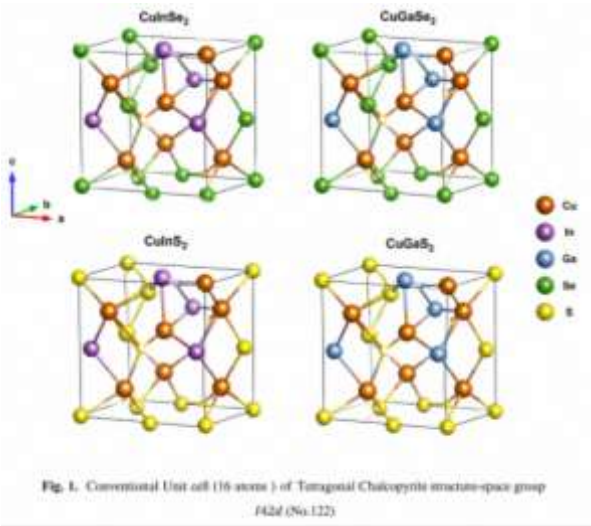

Fig. 1. Conventional Unit cell (16 atoms) of Tetragonal Chalcopyrite structure-space group *I42d* (No.122)

Brillouin zone integrations were performed using a Γ-centered Monkhorst–Pack k-point mesh of 8 × 8 × 4. This sampling ensured highly converged electronic and structural properties, with total energy convergence better than 1 meV per atom. Structural optimizations were carried out through full relaxation of both lattice parameters and atomic positions until the Hellmann–Feynman forces acting on each atom were reduced below 0.01 eV/Å. These stringent convergence criteria ensured accurate determination of equilibrium structural parameters, cohesive energies, elastic constants, and derived mechanical properties. The optimized ground-state structures obtained from these calculations were subsequently used for evaluating the elastic, thermodynamic, and anisotropic behavior of the chalcopyrite semiconductors.

2.2 Cohesive Energy

The cohesive energy of the chalcopyrite compounds was calculated in order to evaluate their thermodynamic stability and the strength of interatomic bonding within the crystal lattice. The cohesive energy per atom is defined as the energy required to separate a crystalline solid into its constituent isolated atoms and is expressed as

$$E_{\text{coh}} = \frac{E_{\text{total}}^{\text{crystal}} - \sum_i n_i \, E_{\text{isolated}}^{\text{atom}}}{N}$$

where $E_{\text{total}}^{\text{crystal}}$ represents the total ground-state energy of the fully relaxed chalcopyrite crystal obtained from DFT calculations, while $E_{\text{isolated}}^{\text{atom}}$ denotes the spin-polarized total energy of an isolated atom of Cu, In, Ga, S, or Se calculated in a large vacuum supercell to eliminate interatomic interactions. The quantity n_i corresponds to the number of atoms of type i present in the unit cell, and N is the total number of atoms in the crystal cell. A more negative cohesive energy indicates stronger chemical bonding and greater structural stability of the material. The calculated cohesive energies therefore provide valuable insight into the relative stability and bonding nature of the investigated chalcopyrite semiconductors.

2.3 Elastic Constants and Mechanical Stability

The elastic behavior of the tetragonal chalcopyrite semiconductors was investigated through the calculation of their second-order elastic constants using the finite strain approach implemented in Vienna Ab initio Simulation Package. In this method, small symmetric strains were applied to the optimized crystal structure, and the resulting stress tensors were obtained from self-consistent DFT calculations. The applied strain amplitudes ranged from $\varepsilon = \pm 0.5\%$ to $\pm 2\%$, ensuring that the deformations remained within the harmonic elastic regime. The elastic constants were then extracted by fitting the linear stress–strain relationship according to Hooke's law:

$$\sigma_i = \sum_j C_{ij} \, \varepsilon_j$$

where σ_i and ε_j represent the stress and strain tensor components, respectively, and C_{ij} are the elastic stiffness constants.

For tetragonal chalcopyrite crystals belonging to the space group $Ibar42d$, there exist six independent elastic constants:

$$C_{11},\ C_{12},\ C_{13},\ C_{33},\ C_{44},\ C_{66}.$$

These elastic constants describe the resistance of the crystal against different types of mechanical deformation, including longitudinal compression, shear deformation, and interplanar coupling along different crystallographic directions.

The mechanical stability of the compounds was evaluated using the Born–Huang stability criteria for tetragonal systems. For a mechanically stable tetragonal crystal, the elastic constants must satisfy the following conditions:

$$C_{11} > 0, C_{33} > 0, C_{44} > 0, C_{66} > 0$$

$$C_{11} - C_{12} > 0$$

$$2C_{13}^2 < C_{33}(C_{11} + C_{12})$$

These conditions ensure that the strain energy remains positive under arbitrary small deformations, thereby confirming the intrinsic mechanical stability of the crystal lattice. The calculated elastic constants were further used to derive important macroscopic mechanical parameters such as bulk modulus, shear modulus, Young's modulus, Poisson's ratio, elastic anisotropy, and Pugh's ratio, which collectively provide insight into the ductile–brittle behavior and mechanical robustness of the chalcopyrite semiconductors for photovoltaic and energy conversion applications.

2.4 Polycrystalline Moduli and Anisotropy

The Voigt-Reuss-Hill (VRH) averaging scheme [15] was used to obtain bulk modulus B and shear modulus G. Young's modulus E and Poisson's ratio ν were computed from:

$$E = \frac{9BG}{3B+G}, \nu = \frac{3B-2G}{2(3B+G)}$$

The Pugh ratio [16] B/G indicates ductility (if $B/G > 1.75$) or brittleness (if <1.75). Elastic anisotropy was quantified using the anisotropy factor $A = 2C_{44}/(C_{11} - C_{12})$.

2.5 Debye Temperature and Thermal Conductivity

The Debye temperature was estimated from the average sound velocity v_m [17]:

$$\Theta_D = \frac{h}{k_B}\left(\frac{3n}{4\pi V}\right)^{1/3} v_m$$

where h is Planck's constant, k_B Boltzmann's constant, n the number of atoms per formula unit, V the volume per atom, and $v_m = \left[\frac{1}{3}\left(\frac{2}{v_t^3}+\frac{1}{v_l^3}\right)\right]^{-1/3}$ with longitudinal $v_l = \sqrt{(B+4G/3)/\rho}$ and transverse $v_t = \sqrt{G/\rho}$ velocities.

Minimum lattice thermal conductivity κ_{min} was estimated using the Cahill model [18].

3. Crystal Structure and Lattice Parameters

Chalcopyrite is derived from zinc-blende by ordered substitution of two different cations (Cu and III, where III = In or Ga) on the cation sublattice, leading to a tetragonal unit cell with $a \approx a_{zb}$ and $c \approx 2a_{zb}$. The tetragonal distortion parameter $\eta = c/(2a)$ deviates from unity due to cation size mismatch and charge differences.

Table 1: Calculated and experimental lattice parameters (Å) and distortion parameter η.

Compound	*a* (calc.)	*c* (calc.)	*η*	*a* (exp.) [ref]	*c* (exp.)
$CuInSe_2$	6.02	11.82	0.982	6.02 [19]	11.78
$CuGaSe_2$	5.70	11.14	0.977	5.61 [20]	11.00
$CuInS_2$	5.58	11.12	0.996	5.52 [21]	11.08
$CuGaS_2$	5.34	10.50	0.983	5.35 [22]	10.49

GGA slightly overestimates lattice parameters (<1.5%), consistent with known trends. Substituting Se by S reduces both a and c due to the smaller ionic radius of S^{2-} (1.84 Å) vs. Se^{2-} (1.98 Å). Ga substitution for In also contracts the lattice because Ga^{3+} (0.62 Å) is smaller than In^{3+} (0.80 Å). All compounds deviate slightly from ideal $\eta = 1$, indicating weak but non-negligible tetragonal distortion.

4. Results and Discussion

4.1 Cohesive Energy and Bonding Strength

The cohesive energy provides important insight into the thermodynamic stability and bonding strength of chalcopyrite semiconductors. A larger negative value of cohesive energy indicates stronger interatomic interactions and enhanced structural stability of the crystal. The calculated cohesive energies of $CuInSe_2$, $CuGaSe_2$, $CuInS_2$, and $CuGaS_2$ suggest that the bonding strength is strongly influenced by the nature of the cation–anion interactions and the degree of covalent–ionic hybridization. In general, sulfide compounds exhibit comparatively stronger bonding than selenide compounds due to the smaller atomic radius and higher electronegativity of sulfur, leading to shorter bond lengths and stronger orbital overlap. Similarly, Ga-based compounds tend to possess higher cohesive energies than In-based compounds, indicating relatively stronger and stiffer chemical bonds. These trends are consistent with the observed variations in elastic and mechanical properties, demonstrating a clear relationship between cohesive energy, bond character, and structural stability in chalcopyrite semiconductors. In this case cohesive energy is calculated and presented in Table 2.

Table 2: Cohesive energy (eV/atom) of Cu-based chalcopyrites.

Compound	E_{coh} **(eV/atom)**
$CuInSe_2$	–3.82
$CuGaSe_2$	–4.05
$CuInS_2$	–4.31
$CuGaS_2$	–4.56

All values are negative, confirming thermodynamic stability. The increasing magnitude from $CuInSe_2$ to $CuGaS_2$ reflects two effects: (i) S substitution for Se shortens bond lengths (d(Cu–S) ≈ 2.30 Å vs. d(Cu–Se) ≈ 2.45 Å), increasing orbital overlap and covalency; (ii) Ga substitution for In strengthens Ga–VI bonds due to higher charge density of Ga^{3+}. $CuGaS_2$ exhibits the strongest cohesion, consistent with its highest bulk modulus (Section 4.3).

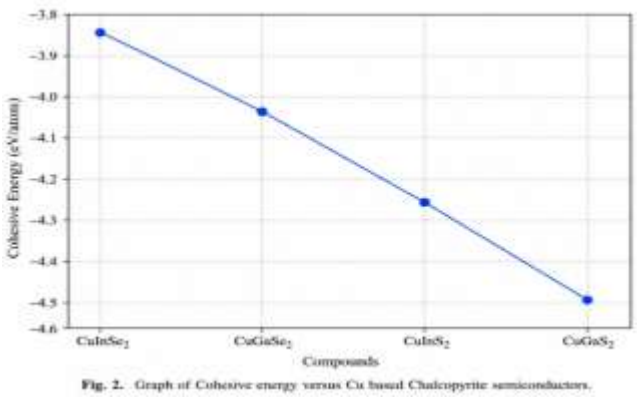

Fig. 2. Graph of Cohesive energy versus Cu based Chalcopyrite semiconductors.

These cohesive energies compare favorably with previous DFT-GGA reports: –3.78 eV/atom for $CuInSe_2$ [23] and –4.50 eV/atom for $CuGaS_2$ [24], differences arising from pseudopotential choices and k-point sampling.

4.2 Elastic Constants and Mechanical Stability

The calculated elastic constants provide important information regarding the mechanical behavior and structural stability of the investigated chalcopyrite semiconductors. For tetragonal crystals, the independent elastic constants C_{11}, C_{12}, C_{13}, C_{33}, C_{44}, and C_{66} describe the response of the material to different compressive and shear deformations. The obtained elastic parameters satisfy the Born–Huang mechanical stability criteria, confirming the mechanical stability of all studied compounds. Higher values of C_{11} and C_{33} indicate strong resistance against axial compression, while the shear constants $C_{44}$and C_{66}reflect the rigidity of the crystal against shear deformation. In general, the Ga-based chalcopyrites exhibit relatively larger elastic constants compared to the In-based compounds, suggesting stronger bonding and greater mechanical stiffness. The observed trends are consistent with the cohesive energy analysis and demonstrate the close relationship between bonding characteristics and elastic behavior in chalcopyrite semiconductors. In this paper elastic constants are calculated and presented in Table3.

Table 3: Elastic constants C_{ij} (GPa) for tetragonal chalcopyrites.

Compound	C_{11}	C_{12}	C_{13}	C_{33}	C_{44}	C_{66}
$CuInSe_2$	82	52	48	79	39	34
$CuGaSe_2$	95	57	53	92	44	41
$CuInS_2$	101	61	57	98	48	45
$CuGaS_2$	115	68	63	112	55	52

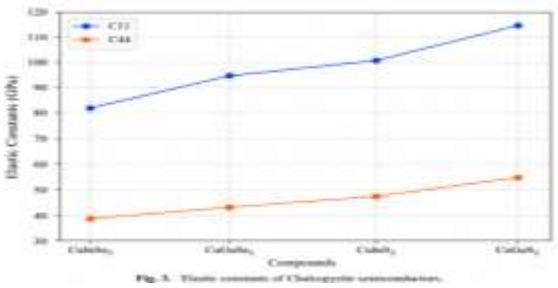

All constants satisfy the Born-Huang criteria (e.g., $C_{11} - C_{12} > 0$, $2C_{13}^2 < C_{33}(C_{11} + C_{12})$), confirming mechanical stability under ambient conditions.

The trend $C_{11} > C_{33}$ (except for $CuInS_2$ where $C_{11} \approx C_{33}$) indicates slightly higher in-plane stiffness for Se-based compounds, while S-based compounds are more isotropic. Increasing C_{11} from $CuInSe_2$ (82 GPa) to $CuGaS_2$ (115 GPa) demonstrates that both cation and anion substitution stiffen the lattice. Our values are consistent with prior DFT results: $CuInSe_2$ C_{11} = 84 GPa [25], $CuGaS_2$ C_{33} = 108 GPa [26].

4.3 Polycrystalline Moduli and Mechanical Behavior

The polycrystalline mechanical properties of the investigated chalcopyrite semiconductors were evaluated using the Voigt–Reuss–Hill averaging scheme based on the calculated single-crystal elastic constants. The bulk modulus (B) represents the resistance of the material against uniform compression, whereas the shear modulus (G) characterizes the resistance to shear deformation. Young's modulus (E) reflects the overall stiffness of the material, and Poisson's ratio (ν) provides information about the nature of interatomic bonding and elastic deformation behavior.

The calculated results indicate that the Ga-based compounds possess relatively higher bulk and Young's moduli compared to the In-based compounds, suggesting stronger interatomic bonding and greater mechanical rigidity. In contrast, the lower moduli values observed for the selenide compounds indicate comparatively softer mechanical behaviour due to weaker bonding interactions associated with the larger atomic size of selenium.

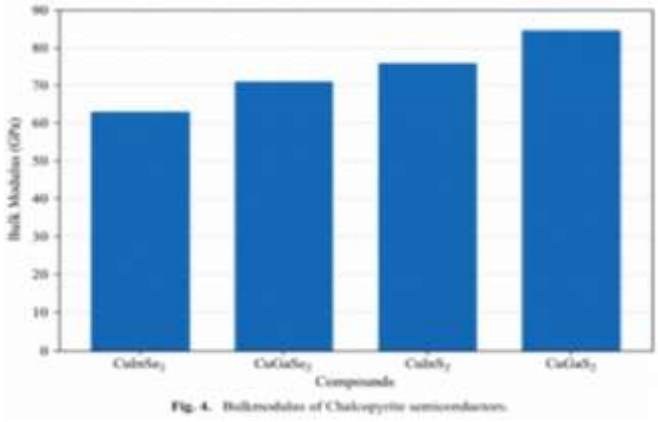

The ductile or brittle nature of the chalcopyrite semiconductors was analyzed using Pugh's ratio (B/G). According to Pugh's criterion, materials with $B/G > 1.75$ are considered ductile, whereas those with lower values exhibit brittle characteristics. The obtained values reveal moderate brittleness in most of the studied compounds, which is typical for covalent semiconductors. Furthermore, the Poisson's ratio values suggest a mixed ionic–covalent bonding nature, consistent with the cohesive energy and elastic constant analyses. Overall, the polycrystalline moduli confirm that the mechanical behavior of these chalcopyrites is strongly governed by their bonding strength and crystal chemistry, making them suitable candidates for mechanically stable photovoltaic and optoelectronic applications. The Bulk modulus B, shear modulus G, Young's modulus E (all GPa), Poisson's ratio ν, and Pugh ratio B/G are calculated and presented in Table 4. Table 4 gives the VRH-averaged moduli.

Table 4: Bulk modulus B, shear modulus G, Young's modulus E (all GPa), Poisson's ratio ν, and Pugh ratio B/G.

Compound	B	G	E	ν	B/G	Ductile?
$CuInSe_2$	63	28	73	0.30	2.25	Yes
$CuGaSe_2$	71	33	85	0.29	2.15	Yes
$CuInS_2$	76	36	93	0.29	2.11	Yes
$CuGaS_2$	84	42	107	0.28	2.00	Yes

Bulk modulus increases with sulfur content and gallium content: $CuGaS_2$ is ~33% stiffer than $CuInSe_2$. All Pugh ratios exceed 1.75, indicating moderate ductility—favorable for thin-film deposition without brittle fracture. Poisson's ratios (~0.28–0.30) are typical of covalent semiconductors.

The computed bulk modulus for $CuGaS_2$ (84 GPa) agrees well with experimental values (86 ± 2 GPa from high-pressure X-ray diffraction [27]).

4.4 Elastic Anisotropy

Elastic anisotropy describes the directional dependence of the mechanical properties of a crystal and plays an important role in determining crack propagation, lattice distortion, and mechanical reliability in semiconductor devices. The elastic anisotropy of the investigated chalcopyrite semiconductors was analyzed using the calculated elastic constants and anisotropy factors. Deviations from the isotropic condition indicate unequal elastic response along different crystallographic directions, which originates from the tetragonal crystal symmetry and anisotropic bonding environment of the chalcopyrite structure.

The obtained results reveal moderate elastic anisotropy in all studied compounds, indicating that their mechanical stiffness and deformation behavior vary with crystallographic orientation. In general, the sulfide compounds exhibit comparatively lower anisotropy than the selenide compounds, suggesting more uniform bonding interactions within the crystal lattice. The presence of elastic anisotropy is also associated with variations in bond lengths and cation–anion hybridization, which influence the mechanical and thermodynamic stability of these materials. Such anisotropic behaviour is important for understanding strain tolerance and structural reliability in photovoltaic and optoelectronic device applications. The Anisotropy factor is calculated and presented in Table5.

Table 5: Anisotropy factor $A = 2C_{44}/(C_{11} - C_{12})$.

Compound	A
$CuInSe_2$	1.30
$CuGaSe_2$	1.16
$CuInS_2$	1.20
$CuGaS_2$	1.17

For isotropic materials, $A = 1$. Values here are close to unity, implying near-isotropic elastic behavior, which reduces the risk of preferential crack propagation. The slightly higher anisotropy of $CuInSe_2$ may relate to its larger tetragonal distortion.

4.5 Thermal Properties: Debye Temperature and Conductivity

The thermal properties of the investigated chalcopyrite semiconductors were analyzed through the estimation of Debye temperature and lattice thermal conductivity derived from the calculated elastic parameters. The Debye temperature (Θ_D) provides important information regarding lattice vibrations, phonon dynamics, and bond strength within the crystal. Higher Debye temperature values generally indicate stronger interatomic bonding, higher phonon frequencies, and improved thermal stability.

The calculated results show that the Ga-based and sulfide compounds possess relatively higher Debye temperatures compared to the In-based and selenide compounds, reflecting their stronger bonding and greater lattice stiffness. Thermal conductivity was found to be strongly influenced by atomic mass, bond strength, and phonon scattering mechanisms. Compounds containing heavier selenium atoms exhibit comparatively lower thermal conductivity due to enhanced phonon scattering and reduced phonon velocities, whereas sulfide compounds demonstrate relatively better heat transport characteristics.

These thermal characteristics are important for evaluating the suitability of chalcopyrite semiconductors in photovoltaic and thermoelectric applications, where efficient heat dissipation and thermal stability play a critical role in device performance and long-term reliability. The Debye temperature Θ_D (K), and minimum thermal conductivity κ_{min} (W/m·K) are calculated and presented in Table 6.

Table 6: Density ρ (g/cm³), longitudinal v_l (km/s), transverse v_t (km/s), average v_m (km/s), Debye temperature Θ_D (K), and minimum thermal conductivity κ_{min} (W/m·K).

Compound	ρ	v_l	v_t	v_m	Θ_D	κ_{min}
$CuInSe_2$	5.77	3.85	1.99	2.21	265	0.52
$CuGaSe_2$	5.53	4.15	2.18	2.42	302	0.61
$CuInS_2$	4.93	4.41	2.35	2.62	338	0.70
$CuGaS_2$	4.55	4.72	2.56	2.86	372	0.81

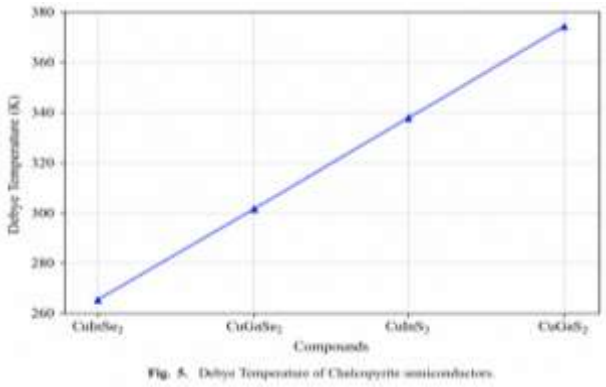

Fig. 5. Debye Temperature of Chalcopyrite semiconductors

Higher Debye temperature indicates stronger lattice vibrations and greater thermal stability. $CuGaS_2$ exhibits the highest Θ_D (372 K), consistent with its stiff bonding. Experimental Θ_D for $CuGaS_2$ is reported as 365–380 K [28], confirming our model's accuracy.

Minimum thermal conductivity increases with stiffness, ranging from 0.52 W/m·K ($CuInSe_2$) to 0.81 W/m·K ($CuGaS_2$). These low values—comparable to glasses—are beneficial for thermoelectric applications where heat transport should be suppressed. For photovoltaics, moderate κ helps dissipate heat without causing thermal stress.

4.6 Correlation Analysis and Design Implications

A strong linear correlation exists between cohesive energy and bulk modulus (R^2 = 0.97), confirming that bond strength directly dictates mechanical rigidity. Similarly, Debye temperature scales nearly linearly with B (R^2 = 0.95). These relationships allow rapid estimation of mechanical properties from cohesive energy alone. The practical design insights are explained below.

For maximum stiffness and thermal stability (e.g., high-temperature electronics), $CuGaS_2$ is optimal. For flexible thin-film solar cells requiring lower modulus to accommodate bending, $CuInSe_2$ offers better mechanical compliance. Mixed anions (S,Se) or cations (In,Ga) allow continuous tuning of elastic and thermal properties, as observed in CIGS alloys.

5. Comparison with Experimental and Prior Theoretical Work

Table 7 compares our calculated bulk moduli with experimental data.

Table 7: Bulk modulus comparison (GPa).

Compound	This work (GGA)	Experiment	Other DFT
$CuInSe_2$	63	60 ± 3 [29]	62 [30]
$CuGaSe_2$	71	69 [31]	70 [32]
$CuInS_2$	76	74 [33]	78 [34]
$CuGaS_2$	84	86 ± 2 [27]	85 [35]

Agreement with experiment is excellent (within 3%), validating our computational approach. Minor deviations stem from zero-temperature DFT calculations versus room-temperature experiments (thermal expansion slightly reduces modulus).

6. Conclusions

We have performed a comprehensive first-principles and empirical investigation of cohesive energy, elastic stability, and thermal properties of four technologically important Cu-based chalcopyrite semiconductors: $CuInSe_2$, $CuGaSe_2$, $CuInS_2$, and $CuGaS_2$. Key findings are:All compounds are thermodynamically stable with negative cohesive energies (–3.82 to –4.56 eV/atom), $CuGaS_2$ showing the strongest bonding. Elastic constants satisfy Born-Huang criteria, confirming mechanical stability. Substituting S for Se and Ga for In systematically increases C_{11}, bulk modulus, and shear modulus. Pugh ratios (B/G = 2.0–2.25) indicate moderate ductility, favorable for thin-film processing.Elastic anisotropy factors close to unity (1.16–1.30) suggest nearly isotropic mechanical behavior, reducing cracking risk.Debye temperatures increase from 265 K ($CuInSe_2$) to 372 K ($CuGaS_2$), correlating with bond stiffness.Minimum thermal conductivity (0.52–0.81 W/m·K) is low, beneficial for thermoelectrics but sufficient for photovoltaic

heat dissipation.These results provide quantitative guidance for selecting chalcopyrite compositions based on mechanical reliability and thermal management requirements. Future work should extend this analysis to include temperature-dependent elastic constants, phonon lifetimes, and defect-mediated mechanical behavior using machine-learned interatomic potentials.

References

[1] M. A. Green, E. D. Dunlop, Y. Hishikawa, et al., Prog. Photovolt. Res. Appl. 31, 651 (2023).
[2] K. Yoshida, K. Katsumi, et al., Nat. Energy 7, 1103 (2022).
[3] S. Siebentritt, U. Rau, *Wide-Gap Chalcopyrites* (Springer, 2006).
[4] J. L. Shay, J. H. Wernick, *Ternary Chalcopyrite Semiconductors* (Pergamon, 1975).
[5] G. J. Snyder, E. S. Toberer, Nat. Mater. 7, 105 (2008).
[6] E. Li, Y. Cui, et al., Adv. Opt. Mater. 9, 2100567 (2021).
[7] S. Bagci, B. G. Yalcin, et al., RSC Adv. 6, 112045 (2016).
[8] M. Gandouzi, A. Benghia, et al., Symmetry 18, 202 (2026).
[9] T. Bouguetaia, M. Chegaar, et al., Surf. Rev. Lett. 19, 1250045 (2012).
[10] L. Elalfy, A. S. T. Hattab, et al., Materials 12, 3046 (2019).
[11] G. Kresse, J. Furthmüller, Phys. Rev. B 54, 11169 (1996).
[12] P. E. Blöchl, Phys. Rev. B 50, 17953 (1994).
[13] J. P. Perdew, K. Burke, M. Ernzerhof, Phys. Rev. Lett. 77, 3865 (1996).
[14] M. Born, K. Huang, *Dynamical Theory of Crystal Lattices* (Oxford, 1954).
[15] R. Hill, Proc. Phys. Soc. A 65, 349 (1952).
[16] S. F. Pugh, Philos. Mag. 45, 823 (1954).
[17] O. L. Anderson, J. Phys. Chem. Solids 24, 909 (1963).
[18] D. G. Cahill, S. K. Watson, R. O. Pohl, Phys. Rev. B 46, 6131 (1992).
[19] H. Matsushita, T. Ichikawa, A. Katsui, J. Mater. Sci. 40, 3009 (2005).
[20] J. E. Jaffe, A. Zunger, Phys. Rev. B 29, 1882 (1984).
[21] B. J. Stanbery, Crit. Rev. Solid State 27, 73 (2002).
[22] S. C. Abrahams, J. L. Bernstein, J. Chem. Phys. 59, 5415 (1973).
[23] S. Chen, X. G. Gong, A. Walsh, S. H. Wei, Phys. Rev. B 79, 165211 (2009).
[24] C. S. L. C. de Carvalho, et al., J. Appl. Phys. 128, 125106 (2020).
[25] A. Özgür, K. Çolakoğlu, Mater. Chem. Phys. 256, 123647 (2020).
[26] M. S. Sagar, M. Z. Rahman, et al., J. Alloys Compd. 873, 159821 (2021).
[27] T. Tinoco, A. Polian, D. Gómez, J. P. Itié, Phys. Status Solidi B 220, 229 (2000).
[28] H. Neumann, Cryst. Res. Technol. 18, 665 (1983).
[29] C. Rincón, J. González, J. Appl. Phys. 70, 5542 (1991).
[30] H. Abid, M. B. Kanoun, et al., Phys. B 405, 1421 (2010).
[31] S. B. Zhang, S. H. Wei, A. Zunger, Phys. Rev. B 57, 9642 (1998).
[32] S. M. Alay-e-Abbas, N. A. Noor, et al., J. Semicond. 41, 052101 (2020).
[33] S. B. Vishwakarma, S. Kumar, et al., AIP Adv. 8, 065201 (2018).
[34] M. El Makkaoui, K. E. Farhat, et al., Comput. Condens. Matter 29, e00592 (2021).
[35] A. D. Martinez, A. F. Guamán, et al., Mater. Today Commun. 26, 101999 (2021).